Investigation of The Coandă Effect in Gas Dynamics Through a First Order Numerical Method

Bereket Guta
Math 406
University of British Columbia

December 17, 2021

Abstract

A first order scheme for the Euler flow within a channel containing a disk is implemented and through a refinement study, first order convergence is observed. The Coandă effect is demonstrated through observations of the magnitude of the velocity around the disk.

1 Introduction

In fluid dynamics, the movement of a compressible, inviscid gas is described well by the Euler equation. These equations are a simplification of the general Naviar-Stokes equations and work only as an approximation to real flows which contain viscosity. In scenarios where lift is to be modeled, these equations are ideal since they provide a good model of reality. Channel flows are a benchmark that are widely used to gain an intuitive understanding to various flows. In this project, we use the deal-ii package to simulate a pipe flow around a disk. Through these simulations, the Coandă is modeled. This effect is the tendency for a fluid coming from an opening to follow an adjacent flat or curved region and thus create a region of low pressure.

2 Background

Using the work of [1] as the basis of for this approach, the Euler equation for a compressible fluid is

$$\frac{\partial \mathbf{u}}{\partial t} + \nabla \cdot \mathbf{f}(\mathbf{u}) = 0 \tag{1}$$

where for a dimension $d \geq 1$,

$$\begin{aligned} \mathbf{u}(\mathbf{x}, t) &: \mathbb{R}^d \times \mathbb{R} \to \mathbb{R}^{d+2} \\ \mathbf{f}(\mathbf{u}) &: \mathbb{R}^{d+2} \times \to \mathbb{R}^{d+2} \times \mathbb{R}^d \\ \mathbf{u} &= [\rho,\ \mathbf{m},\ E]^T \\ \mathbf{f}(\mathbf{u}) &= \begin{bmatrix} \mathbf{m}^T \\ \mathbf{v} \otimes \mathbf{m} + \mathbb{I}p \\ \mathbf{v}^T(E+p) \end{bmatrix} \end{aligned}$$

$\rho \in \mathbb{R}^+$ is the density, $\mathbf{m} \in \mathbb{R}^d$ the momentum, $E \in \mathbb{R}^+$ the total energy of the system, $\mathbf{v} = \rho^{-1}\mathbf{m}$ is the velocity and p the pressure. Assuming the gas is polytropic and ideal, the pressure is defined by the equation of state

$$p(\mathbf{u}) = (\gamma - 1)(E - \frac{1}{2}\rho|\mathbf{v}|^2)$$

where $\gamma \in [1, \frac{5}{3}]$ is the ratio of the specific heats which is assumed to be 1.4.

3 Method

The structure of the implementation of the solution uses the work of [3] as a foundation. Hyperbolic equations of the form 1 are difficult to solve due to their non-linearity. For a solution $\mathbf{u}$ to be physical, a constraint can be imposed such that any solution must be contained in the invariant set of Euler's equations. This set, $\mathcal{B}$, is

$$\mathcal{B} = \{\mathbf{u} \,|\rho > 0,\ E - \frac{1}{2}\rho|\mathbf{v}|^2 > 0,\ s(\mathbf{u}) \geq \min_{\mathbf{x}} s(\mathbf{u}_0(\mathbf{x}))\}$$

where s is the specific entropy

$$s(\mathbf{u}) = \log[\frac{p(\mathbf{u})}{\rho}].$$

This indicates that for the solution to represent a physical system, there must be a local minimum principle on the specific entropy in addition to a positive value for both density and internal energy. Violations of this constraint leads to non-physical solutions which implies that any numerical scheme must satisfy this constraint. Due to the success of finite-difference and finite volume schemes, a similar scheme is implemented such that the pointwise constraint is satisfied

$$\forall \mathbf{x}_i \in \Omega,\ u_h(\mathbf{x}_i, t) \in \mathcal{B}.$$

The scheme solves $u_h = \sum_i U_i \phi_i$ using

$$m_i \frac{\mathbf{U}_i^{n+1} - \mathbf{U}_i^n}{\Delta t} + \sum_{j \in I(i)} \mathbf{f}(\mathbf{U}_j^n) \cdot \mathbf{c}_{ij} - \sum_{j \in I(i)} d_{ij}(\mathbf{U}_j^n) = 0.$$

Where $m_i = \int_\Omega \phi_i d\mathbf{x}$ is the mass matrix, $\mathbf{c}_{ij} = \int_\Omega \nabla\phi_j \phi_i d\mathbf{x}$ the flux, $I(i)$ contains all nonzero column indices of $\mathbf{c}_{ij}$ for row index i and

$$d_{ij} = \max\{\lambda_{\max}(\mathbf{U}_i^n, \mathbf{U}_j^n, \mathbf{n}_{ij}), \lambda_{\max}(\mathbf{U}_j^n, \mathbf{U}_i^n, \mathbf{n}_{ji})\}\|\mathbf{c}_{ij}\|$$

$$d_{ii} = -\sum_{j \in I(i)|i} d_{ij}$$

is the local viscosity where $\mathbf{n}_{ij} = \frac{\mathbf{c}_{ij}}{\|\mathbf{c}_{ij}\|}$ and $\lambda_{\max}$ is the maximum local wavespeed as defined in [2] which is computed using a Riemann solver. For the boundary conditions, an inflow and outflow condition are specified on the left and right sides while the no slip condition is enforced on the top and bottom surfaces of the domain. The CFL condition is maintained for

$$\Delta t_n = c_{\text{cfl}} \min_{i \in \mathcal{V}} \left(\frac{m_i}{-2\, d_{ii}^n} \right),$$

where c_{cfl} is taken to be 0.8.

4 Results

To test performance of this scheme a refinement study is conducted and the forces on a disk submerged in the fluid are observed. For the refinement study a channel of length 4 and height 2 is used. The disk is placed at the origin with a diameter of 0.5, the left side of the domain is a distance of 0.6 from the center of the the disk. During refinement each cell within the mesh 1 is split into two. The values for density are calculated at various points and compared across the refined meshes. The mesh 2, created after $N = 5$ divisions of the grid, is considered to be the ground truth. The error is calculated as

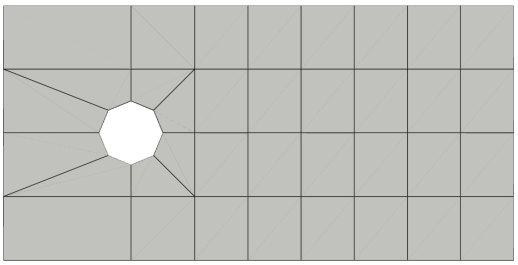

Figure 1: Initial mesh used in the refinement study. This mesh is composed of three separate rectangles.

$$E_N = |\rho_N(\mathbf{x}) - \rho_5(\mathbf{x})|$$

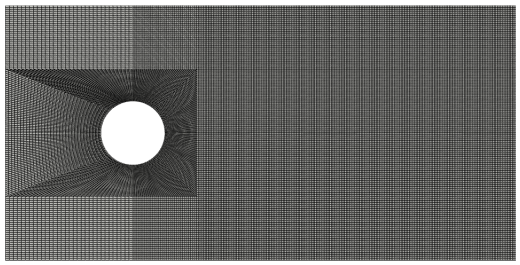

Figure 2: The final mesh used in the refinement study. This is generated by splitting each cell in 1 into 2 five times.

for $N < 5$. A uniform flow in the x direction with a value of 1 is used throughout the experiment. The initial conditions are set uniformly with a value of 1.4 for initial density, 3 for the initial velocity, 1 for the pressure. The total run time for the simulation is three seconds. The log of the inverse error is plotted below to show convergence.

From figures 3, 4 and 5 first order convergence is observed. This pattern is seen for most points in the mesh but positions in front of the disk at a distance less than -0.45 in the x direction deviated from this convergence. Figure 6 shows that a finer mesh is needed to observe convergence.

To demonstrate the Coandă result, the flow in time is plotted. Due to the symmetry of the flow a net torque of zero is observed as the forces balanced out on the top and bottom. In reality, asymmetry would lead to a non-zero net torque. The effect is clearly visible due to the velocity gradient between the sides and front of the disk. This indicates that the flow is slowing down as it curves around the disk. Snapshots of this effect at various times are plotted.

From figures 7 to 13, the curvature of the flow follows the curvature of the disk. A splitting effect is observed at the

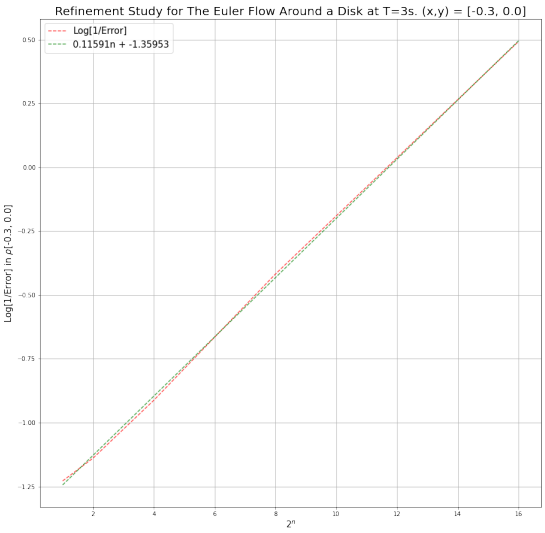

Figure 3: Refinement study for the point $(-0.3, 0)$ which is in front of the disk. First order convergence is observed as the number of grid points increased.

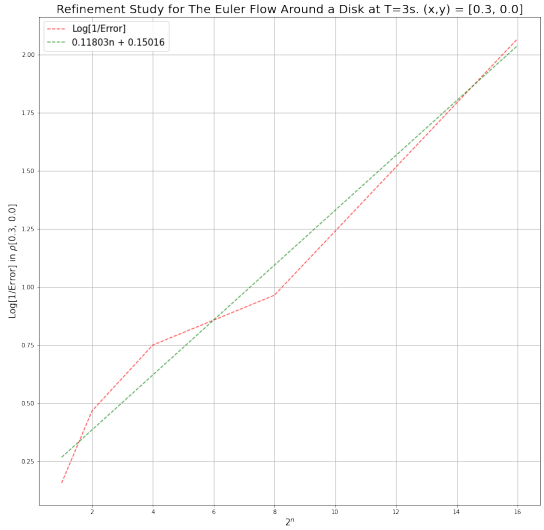

Figure 4: Refinement study for the point $(0.3, 0)$ which is located behind the disk. First order convergence is observed as the number of grid points increased. The convergence here is not as clean as the 4.

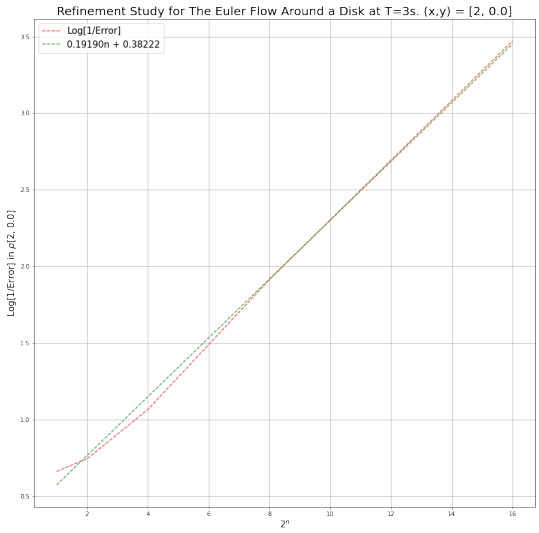

Figure 5: Refinement study for the point $(2, 0)$ which is located far behind the disk. First order convergence is observed as the number of grid points increased.

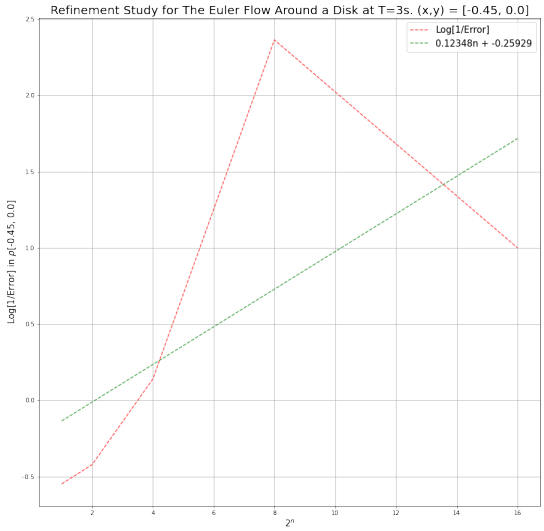

Figure 6: Refinement study for the point $(-0.45, 0)$ which is located in front of the disk. Points at and further (more negative) than this point lacked the first order convergence.

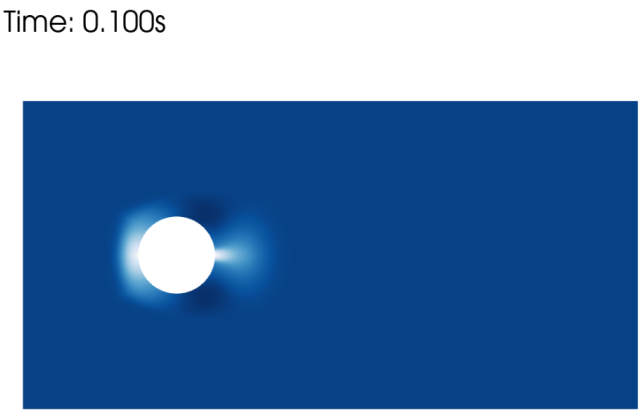

Figure 7: Velocity magnitude plot for the flow around the disk for mesh 2. Lighter colors indicate larger intensity.

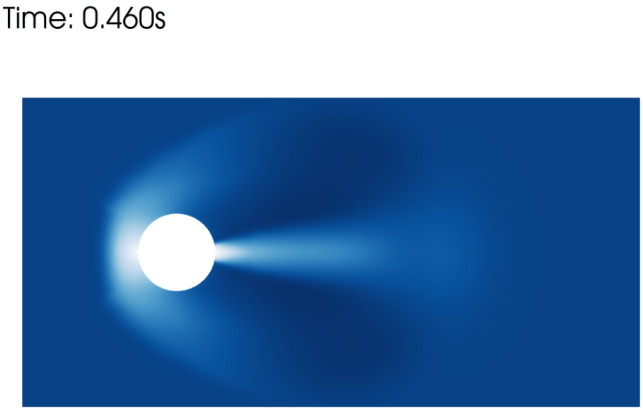

Figure 8: Velocity magnitude plot for the flow around the disk for mesh 2. Lighter colors indicate larger intensity.

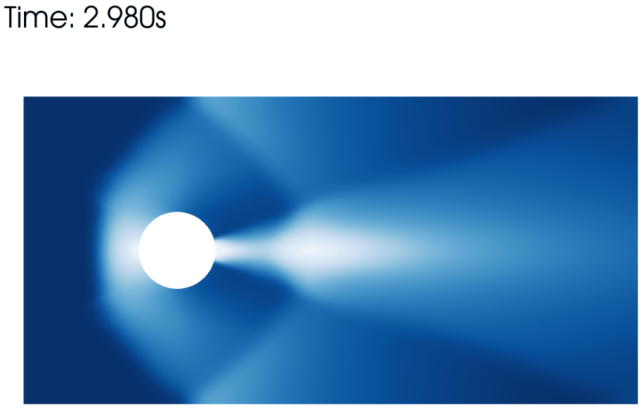

Figure 9: Velocity magnitude plot for the flow around the disk for mesh 2. Lighter colors indicate larger intensity.

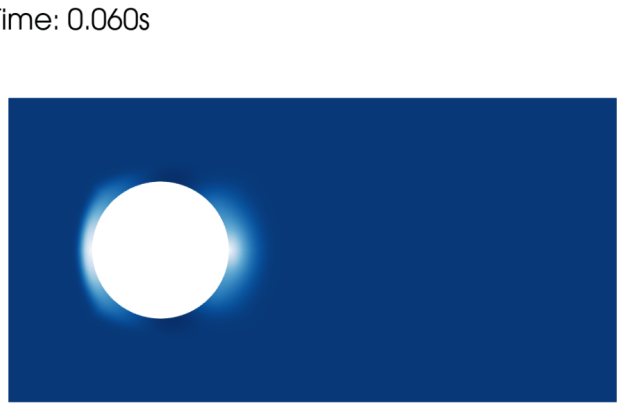

Figure 10: Velocity magnitude plot for the flow around the disk with a diameter of 0.9. Lighter colors indicate larger intensity.

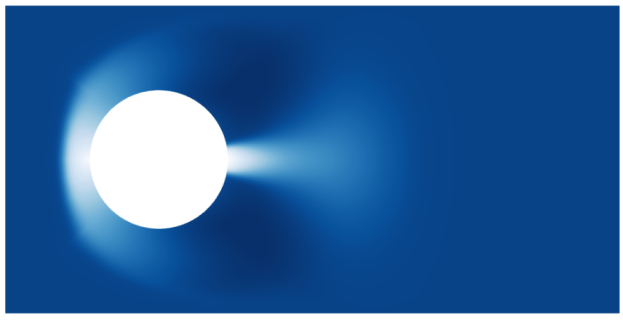

Figure 11: Velocity magnitude plot for the flow around the disk with a diameter of 0.9. Lighter colors indicate larger intensity.

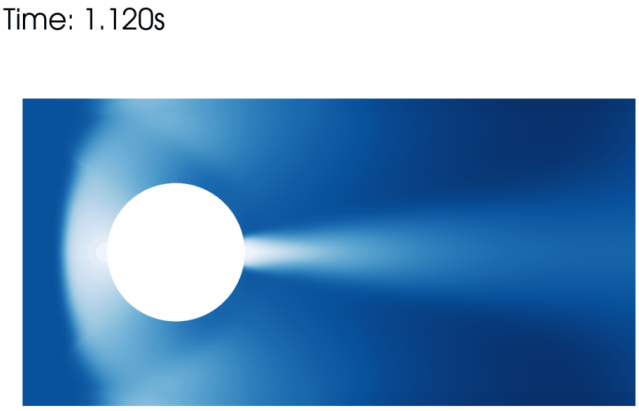

Figure 12: Velocity magnitude plot for the flow around the disk with a diameter of 0.9. Lighter colors indicate larger intensity.

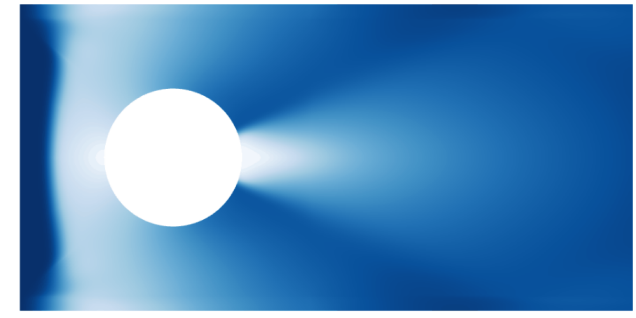

Figure 13: Velocity magnitude plot for the flow around the disk with a diameter of 0.9. Lighter colors indicate larger intensity.

front of the disk where impact occurs. From this split the fluid flows symmetrically around and slows down as it remains attached to the surface. A speed up is seen again as the two curves meet back up at the other side.

5 Conclusion

The Coandă effect is observed whenever a fluid encounters a curved surface. The demonstration of the flow of a fluid described by the Euler equations around a disk indicates that the flow curves in the same way the Coandă effect explains. Through refinement studies first order convergence is observed. Convergence of this order is impractical as it requires the use of many grid points and is computationally intensive. Other practical approaches exist but this method showcases the interesting qualities of the Naviar-Stokes model.

References

[1] Jean-Luc Guermond, Matthias Maier, Bojan Popov, and Ignacio Tomas. Second-order invariant domain preserving approximation of the compressible navier–stokes equations. *Computer Methods in Applied Mechanics and Engineering*, 375(1):113608, 2021.

[2] Jean-Luc Guermond and Bojan Popov. Invariant domains and first-order continuous finite element approximation for hyperbolic systems. *SIAM J. Numer. Anal.*, 54:2466–2489, 2016.

[3] Matthias Maier and Ignacio Tomas. tamiko/step-69: step-69 v20200305, 2020.